Experimental study of potassium release during biomass-pellet combustion and its interaction with inhibitive additives

Yingzu Liu[1], Kaidi Wan[2,*], Yong He[1,*], Zhihua Wang[1], Jun Xia[3], Kefa Cen[1]

1. State Key Laboratory of Clean Energy Utilization,

Zhejiang University, Hangzhou 310027, China

2. CORIA – CNRS, Normandie Université,

INSA de Rouen, 76800 Saint-Etienne-du-Rouvray, France

3. Department of Mechanical and Aerospace Engineering & Institute of Energy Futures,

Brunel University London, Uxbridge UB8 3PH, UK

* Corresponding authors: kaidi.wan@coria.fr (Kaidi Wan); heyong@zju.edu.cn (Yong He).

Abstract

In the present study, two types of biomass were investigated as typical agricultural and woody biomass fuel, i.e., corn straw and poplar. Firstly, laser induced breakdown spectroscopy (LIBS) was employed to investigate the release characteristics of potassium (K) from a burning biomass pellet. In order to further investigate the correlation between K release and the combustion process, combustion parameters including pellet surface temperature and pellet diameter were simultaneously measured with LIBS. A dual-peak trend is observed in the K release history of poplar, but only a single peak is found in that of corn straw. Both biomass samples show the strongest K release during the devolatilization stage in comparison with the subsequent char burnout and ash cooking stages. Similar tendencies are observed between K release and pellet temperature, which suggests that K release is closely related to the combustion process. The K release mechanism can be attributed to temperature rise and therefore breakdown of chemical bonds during combustion. Then the release of different chemical forms of K was investigated by chemical fractionation treatment of the biomass samples.

The released amount of H_2O-soluble, NH_4Ac-soluble and HCl-soluble potassium compounds were obtained. The H_2O-soluble potassium is found to be the major released potassium compound. Finally, four kinds of additives (two pure additives, i.e., silica and alumina, and two typical natural mineral additives, i.e., kaolin and mica) were added to the biomass samples to investigate their inhibition effects on K release. The natural sorbent additives show better inhibition effects than the pure ones.

Keywords: Potassium; LIBS; Fractionation; Inhibition; Biomass

1. Introduction

Biomass, as a renewable energy source, has been utilized to support 10–15% of the worldwide energy consumption [1], especially with soaring applications in thermal power production. However, advanced thermo-utilization of biomass is largely limited by severe ash deposition issues caused by alkali metal emissions [2]. Since potassium (K) is an important element for plants, it is usually rich in biomass. The potassium vapor released during the thermo-utilization of biomass tends to condense on cooler heat exchange surfaces and develop a sticky potassium layer. The sticky layer could capture fly ash and then result in ash deposition [3, 4]. Moreover, potassium could also react with sulfur and chlorine species, leading to severe fouling and corrosion [5, 6]. It is therefore important to understand potassium-release mechanisms during biomass combustion in order to develop potassium control technologies and achieve better utilization of biomass resources [7-10].

In the past few decades, experimental study on potassium release characteristics during biomass combustion has evolved from offline sampling approaches to online in-situ measurements using optical techniques [11-13]. These non-intrusive optical techniques can directly capture dynamic

47 potassium-release characteristics during biomass combustion. For instance, flame emission
48 spectroscopy method has been employed to investigate potassium release characteristics [11] and the
49 effects of different combustion atmosphere on potassium release [14] during biomass combustion.
50 Weng et al. [15] measured the release of atomic potassium from burning coal, wood, and straw pellets
51 using tunable diode laser absorption spectroscopy (TDLAS). Qu et al. [16] used the same technique to
52 simultaneously measure the flame temperature, water vapor and atomic potassium distribution during
53 entrained-flow biomass combustion and they observed that potassium species rapidly undergo primary
54 ash transformation reactions even if the fuel particles reside in an oxygen-deficient environment. Other
55 laser optical diagnostics techniques have also been used, including collinear photo-fragmentation
56 atomic absorption spectroscopy (CPFAAS) [17], laser induced fragmentation fluorescence (ELIF) [18],
57 laser-induced breakdown spectroscopy (LIBS) [19] and planar laser-induced fluorescence (PLIF) [20].
58 In order to obtain the potassium proportion in solid residues, inductively coupled plasma-optical
59 emission spectrometry (ICP-OES) is usually employed [21] to measure the remaining elemental
60 potassium. Very recently, Liu et al. [22] used ICP-OES to investigate the effects of atmosphere and
61 chlorine on potassium release during biomass combustion in a fluidized bed and the results show that
62 the release proportion of potassium in air atmosphere was bigger than oxy-fuel environment and the
63 overall activation energy for potassium release under air atmosphere is less than that under oxy-fuel
64 atmosphere.

65 From previous studies [2, 23], we know that potassium compounds in biomass can be classified
66 into four groups: (1) H_2O-soluble potassium, which exists as potassium salts, e.g., potassium chloride;
67 (2) CH_3COONH_4 (NH_4Ac)-soluble potassium, which is bounded to carboxyl groups; (3) HCl-soluble
68 potassium, which is organically bounded to functional groups containing oxygen or nitrogen; (4)

69 insoluble potassium, which is attached to minerals. NH_4Ac- and HCl-soluble potassium compounds
70 together are also referred to as organically-bound potassium. The release characteristics of individual
71 forms of potassium compounds have been investigated mainly via offline inductively coupled plasma
72 (ICP) measurements. For instance, Deng et al. [24] studied the transformation of different forms of
73 potassium compounds during rapid pyrolysis of wheat straw, corn stalk and rice hull under different
74 temperatures. On the other hand, numerical methods have also been utilized to investigate the release
75 of different forms of potassium [25], e.g., the first order Arrhenius expression model [26], the two-step
76 kinetics model [20] and even the two-step kinetics release model combined with the gas phase
77 potassium transformation kinetics [27], although some key information such as the time-resolved
78 release history of different forms of potassium are still lack for a complete model validation. To the
79 authors' best knowledge, the online dynamic release characteristics of different forms of potassium
80 compounds during biomass combustion have not been revealed yet.

81 To reduce harmful potassium emissions, inhibition technologies can be used and classified into
82 the following two categories: (1) pretreatment by water washing to remove potassium before
83 combustion [28] and (2) addition of potassium sorbent additives to inhibit potassium release during
84 combustion [29]. While both approaches have shown their potential to alleviate ash deposition and
85 corrosion in biomass-fired furnaces, the additive approach appears more advantageous in that it saves
86 water and the additives can be directly injected into boilers without any major reconfiguration.
87 Previous studies on inhibition additives of potassium release have shown that additives with a high
88 content of Al or Si are effective to reduce potassium release [29, 30]. For example, Mason et al. [29]
89 used flame emission method to investigated the effects of an aluminosilicate based additive on the
90 release of potassium during biomass pellets combustion and the results suggest that high chlorine

and/or low (Si+Al) facilitates the release of KCl or KOH to the gas phase, while high (Si+Al) helps to keep K in the solid phase. To achieve a deeper understanding of the inhibition mechanism of various additives, however, the potassium-release dynamics that interacts with these additives during biomass combustion are still required.

In order to bridge these research gaps and achieve a better understanding of the release characteristics of different forms of potassium compounds and the inhibition mechanisms of different additives, the present study employs the LIBS technique to obtain time-resolved profiles of potassium released from a burning biomass pellet mixed with four different additives. In addition, offline ICP analyses are performed along with the chemical fractionation method to reveal the transformation of different chemical forms of potassium compounds in the solid phase. A combination of online and offline measurements can provide us comprehensive physical insights into potassium release during biomass combustion and its interaction with inhibitive additives.

2. Experimental methods

2.1. Biomass samples and mineral additives

Two biomass fuels, corn straw and poplar, have been used, which are representative agricultural and woody type biomass, respectively. The results of the proximate analysis, ultimate analysis and also the ash compositions of the two biomass samples are summarized in Table 1. The proximate analysis was determined via chemical analysis methods according to the Chinese National Standard GB/T 212-2008. The ultimate analysis was performed according to the Chinese National Standard GB/T 476-2008 (for carbon and hydrogen), GB/T 19227-2008 (for nitrogen) and GB/T 214-2007 (for sulfur). The mass fraction of oxygen was then calculated based on mass balance, i.e., $O_{daf}\% = 100\% - C_{daf}\%$

– H_{daf}% – N_{daf}% – S_{daf}%. Ash compositions were obtained according to the Chinese National Standard GB/T 1574-2007. One of the four additives was blended with the biomass samples to investigate their inhibition effects on potassium release. Specifically, two pure additives, i.e., silica and alumina, and two natural mineral additives, i.e., kaolin and mica, were employed. Table 2 gives the physical and chemical properties of the four additives. All the additives were blended with the biomass at a dosing ratio of 3% by weight, which is a typical dose for sorbents [31, 32]. To ensure the additives were well mixed with the biomass, both the additives and biomass were first grounded and sieved to fine powder with a diameter less than 75 μm. Then they were mixed in a grinder of 32,000 rpm for 5 minutes to obtain blended biomass-additive powders.

Table 1. Chemical analyses of biomass samples.

	Proximate analysis (wt.%)				Ultimate analysis (wt.%)				
	M_{ad}	A_{ad}	V_{ad}	FC_{ad}	C_{daf}	H_{daf}	N_{daf}	S_{daf}	O_{daf}
Corn Straw	11.6±0.22	7.9±0.12	64.2±1.27	16.3±0.42	43.9±0.94	4.5±0.09	1.8±0.06	0.4±0.09	49.3±1.03
Poplar	11.6±0.19	2.3±0.05	66.3±1.69	19.8±0.39	45.9±0.87	4.1±0.06	0.7±0.05	0.1±0.03	49.2±1.28

	Ash analysis (wt.%)								Cl_{ad}	K_{ad}	P_{ad}
	SiO_2	Al_2O_3	Fe_2O_3	CaO	MgO	K_2O	Na_2O		mg/g	mg/g	mg/g
Corn Straw	47.52±1.10	5.64±0.29	1.04±0.17	4.51±0.38	12.6±0.72	7.87±0.77	1.97±0.14	Corn Straw	1.34±0.12	13.1±0.79	0.7±0.11
Poplar	30.97±0.89	5.09±0.37	2.6±0.21	29.32±0.92	5.96±0.42	6.94±0.85	2.9±0.17	Poplar	1.04±0.11	7.09±0.61	<0.1

Table 2. Physical and chemical properties of the additives.

	Silica	Alumina	Kaolin	Mica
Dimensional parameter				
Surface area (m^2/g)	0.3	173	7.8	3.1
Pore volume (cm^3/g)	0.002	0.244	0.037	0.012
Mean pore diameter (nm)	18.6	5.6	18.7	16.2
Chemical composition (wt %)				
Al_2O_3		>99	21.54±0.79	25.54±0.99
SiO_2	>99		66.64±1.57	65.49±1.77
Na_2O			0.18±0.01	0.73±0.04
CaO			0.12±0.01	0.18±0.02
MgO			0.43±0.02	2.06±0.19
Fe_2O_3			0.27±0.02	2.25±0.21
K_2O			0.19±0.02	5.24±0.39

2.2. Identification of the chemical forms of potassium

Different chemical forms of potassium can be identified according to their solubility in different solvents through a chemical fractionation method. First, 1 gram of the biomass sample was added into 100 ml water at 333 K, and the solution was stirred for 24 hours before a filtering operation is applied. The content of the H_2O-soluble potassium such as potassium sulfates and chlorides can be determined by using inductively coupled plasmas-atomic emission spectroscopy (ICP-AES) to analyze the filtrate. The solid filter residue was then sequentially dissolved in 100 ml NH_4Ac (1 mol/L) and 100 ml HCl (1 mol/L). The filtrate of each step was analyzed with ICP-AES to identify NH4Ac-soluble and HCl-soluble potassium. The final residual following HCl extraction was dissolved in strong acid and then analyzed with ICP-AES to determine the content of the insoluble potassium, such as potassium silicate.

The solid filter residuals obtained in each step, with H_2O-soluble, NH_4Ac-soluble, and HCl-

soluble potassium sequentially removed, were dried in an oven at 333 K for 24 h before further use.

2.3. LIBS measurement system

The setup of the LIBS measurement system is shown in Fig. 1. A 4 mm spherical pellet was suspended on two ceramic rods (diameter of 1 mm) at a height of 10 mm above a heat flux burner. The pellet was produced by pressing 50 mg fuel powder, which are pulverized biomass, biomass-additive mixture or the solid filter residuals obtained in the chemical fractionation treatment. The maximum pressure used in the fabrication of the pellets could reach 2.5 MPa. The burner generated a laminar premixed methane-air flame at an equivalence ratio of 0.8. The flow rates of methane and air were 0.59 SL/min and 7.06 SL/min, respectively. The flame was simulated using CHEMKIN with the GRI-3.0 mechanism [33]. The temperature at the pellet height was predicted to be 1892 K, and the major species compositions are 72.8% N_2, 3.9% O_2, 7.6% CO_2 and 15.4% H_2O in mass.

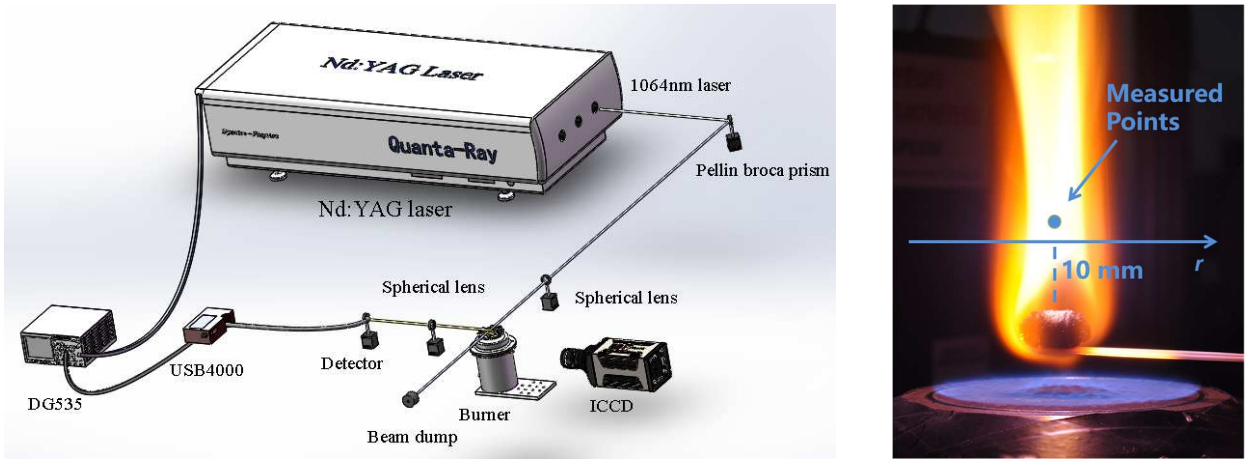

(a) Configuration of equipment (b) Measured location

Figure 1. LIBS measurement setup.

An Nd:YAG laser (Spectra Physics, model PRO-250) with a fundamental wavelength of 1064 nm was focused into the gas plume at 10 mm above the burning pellet. The repetition rate, pulse duration

and average energy of the laser were 10 Hz, 10 ns and 300 mJ, respectively. An Ocean Optics spectrometer (model USB 4000) was employed to collect the LIBS signal. The laser and the spectrometer were synchronized using a digital pulse generator (Stanford Research System, model DG535).

To measure the quantitative potassium concentration, the LIBS signal was calibrated by measuring the potassium spectral intensity (769.9 nm) for a potassium chloride (KCl) seeded flame of a known concentration of potassium. The detailed calibration procedure can be found in our previous study [34]. The obtained linear response of the LIBS signal to the potassium concentration is:

$$I_{\mathrm{LIBS,K}} = 1927 C_{\mathrm{K}},\ R^2 = 0.97 \quad (1)$$

where $I_{\mathrm{LIBS,K}}$ is the LIBS signal intensity (-), C_{K} is the potassium concentration (mg/m^3) at the measuring point, and R^2 is the coefficient of determination (-). The measurement uncertainties of the LIBS system can be attributed to laser energy fluctuation, calibration uncertainty and electronic noise. Base on the maximum error of calibration and measurement standard deviation, the maximal error values of the K release rates are (a) Poplar: ±4.1e-4 mg/s (±15.3%); (b) Corn Straw: ±1.8e-3 mg/s (±12.7%). The readers could refer to [20] for more detailed analyses on the experimental uncertainties.

2.4. Optical measurement for the temperature and diameter of a pellet

The surface temperature of a burning pellet was measured using a two-color pyrometer [35]. The response of the two-color pyrometer, $I_{(\lambda,T)}$, is proportional to the radiant exitance of the measured pellet surface [36]:

$$I_{(\lambda,T)} = R_c \times S_\lambda \times \varepsilon_\lambda \times \frac{C_1}{\lambda^5} \times e^{-C_2/(\lambda T)}, \quad (2)$$

where R_c is an instrument constant [37], S_λ is the spectral sensitivity of the charge coupled device

(CCD), ε_λ is the monochromatic emissivity, T is the pellet surface temperature (K), and C_1 and C_2 are the first and second Planck's constants. By using Wien's equation to compare $I_{(\lambda,T)}$ at two different wavelengths, the pellet surface temperature can be calculated as [36]:

$$T = \frac{C_2\left(\frac{1}{\lambda_2}-\frac{1}{\lambda_1}\right)}{\ln\frac{I_{\lambda_1}}{I_{\lambda_2}}+\ln\frac{S_{\lambda_1}}{S_{\lambda_2}}+\ln\frac{\varepsilon_{\lambda_1}}{\varepsilon_{\lambda_2}}+\ln\frac{\lambda_1^5}{\lambda_2^5}} \quad . \tag{3}$$

The value of $S_{\lambda1}/S_{\lambda2}$ was calibrated using a thermocouple in the flame produced by the heat flux burner, for the purpose of correcting the spectral response of both the CCD and filters.

In the present study, a bioptic lens attachment (model LAVISION VZ-image doubler) is employed to capture two-dimensional (2D) images of a pellet at 1 Hz. Two filters with a bandwidth of 1 nm, which are centered at 633 nm and 647 nm, provide the spectral discrimination required for the two-color pyrometry. Because the two wavelengths are close to each other, $\varepsilon_{\lambda1}/\varepsilon_{\lambda2}$ is approximately unity.

The shape of a burning pellet can be obtained from the 2D images of thermal irradiation [38]. The diameter of the pellet is then computed as the average of two orthogonal dimensions in each image.

3. Results and discussion

3.1. Potassium release characteristics of poplar and corn straw

Temporal potassium release profiles of burning poplar and corn straw pellets measured by the LIBS technique are shown in Fig. 2. Each measurement was repeated three times and the average result is shown along with error bars indicating the statistical uncertainty of the measurements. A three-stage release characteristics of potassium can be clearly observed for the poplar, which is similar to our previous finding on the sodium release characteristics of a burning coal pellet [32, 39]: (1) the first narrow peak appears during the devolatilization stage; (2) then a second wider peak occurs during the

char burnout stage; (3) finally, the potassium concentration slowly decreases to the baseline in the ash cooking stage. The three stages in Fig. 2 are separated according the method previously reported in [35]. For the corn straw, however, only one peak of the potassium concentration can be found in the devolatilization stage. Therefore, the second char burnout stage and the third ash cooking stage cannot be separated due to the lack of a second peak. Besides, the char burnout stage of corn straw features a monotonic decreasing profile of K concentration instead of a wide peak observed in that of poplar, which could be due to an overlap between the devolatilization and char burnout stages for corn straw. It indicates the char oxidation of the corn straw pellet proceeds in a different manner than that of poplar or coal combustion [20]. The kinetics and mechanism of char burnout may be different for poplar and corn straws due to their different fuel compositions and structures. From the ultimate analysis in Table 1, the oxygen to carbon ratio is 1.123 for corn straw while 1.072 for poplar, which means poplar has a higher fuel rank than corn straw, i.e., poplar is closer to coal while corn straw is closer to agricultural biomass. As reported in [5], adding biomass to coal could leads the char burnout stage shifts towards an earlier time and get merged with the devolatilization stage.

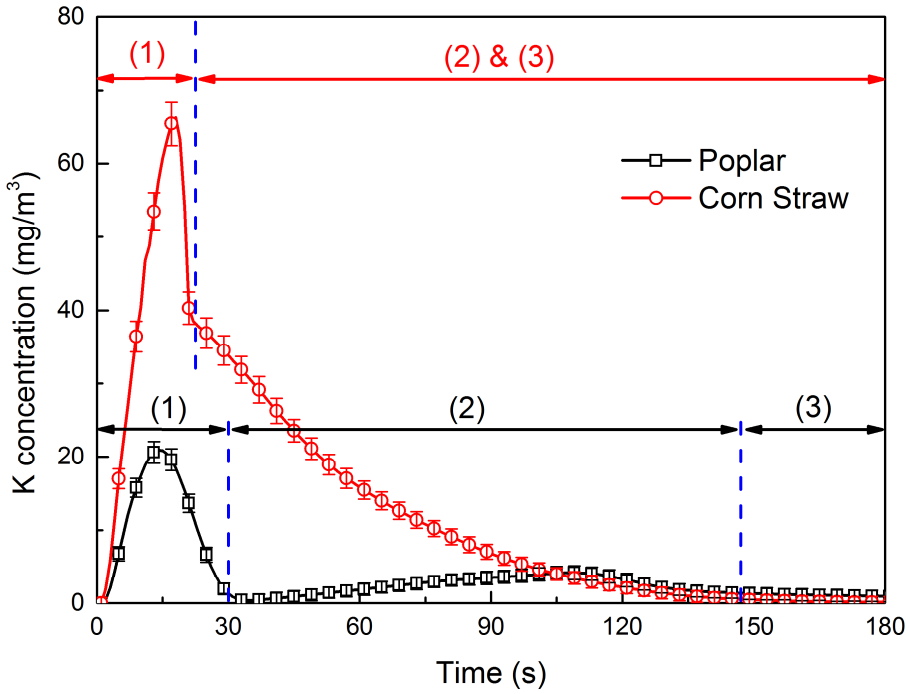

Figure 2. Temporal potassium release profiles of poplar and corn straw measured by LIBS. The three combustion stages of the biomass pellets are: (1) devolatilization, (2) char burnout, and (3) ash cooking.

Figure 3 shows temporal profiles of the surface temperature (T) of the poplar and corn straw pellets. Similar to the profiles of potassium release, the surface temperature profiles of the two biomass samples are also different, with a dual-peak profile for poplar while a single-peak one for corn straw. The dual-peak profile of poplar is similar to what has been observed in a burning coal pellet [39, 40]: (1) in the first devolatilization stage, the pellet is rapidly heated by the high-temperature coflow and volatile is released, leading to a volatile flame surrounding the pellet. The burning of volatile further heats the pellet and leads to the first peak of the surface temperature; (2) since the heating effect of the volatile flame disappears, the pellet slightly cools down. Then the thermal effect of char oxidization heats the pellet again and results in the second peak of the surface temperature of poplar; (3) the residual incombustible ash of the pellet achieves thermal equilibrium with the surrounding coflow. The single-peak characteristic of corn straw is consistent with its potassium release profile, which suggests

231 a mild char oxidation as the pellet surface temperature gradually decreases towards the equilibrium
232 temperature during the char and ash stages.
233

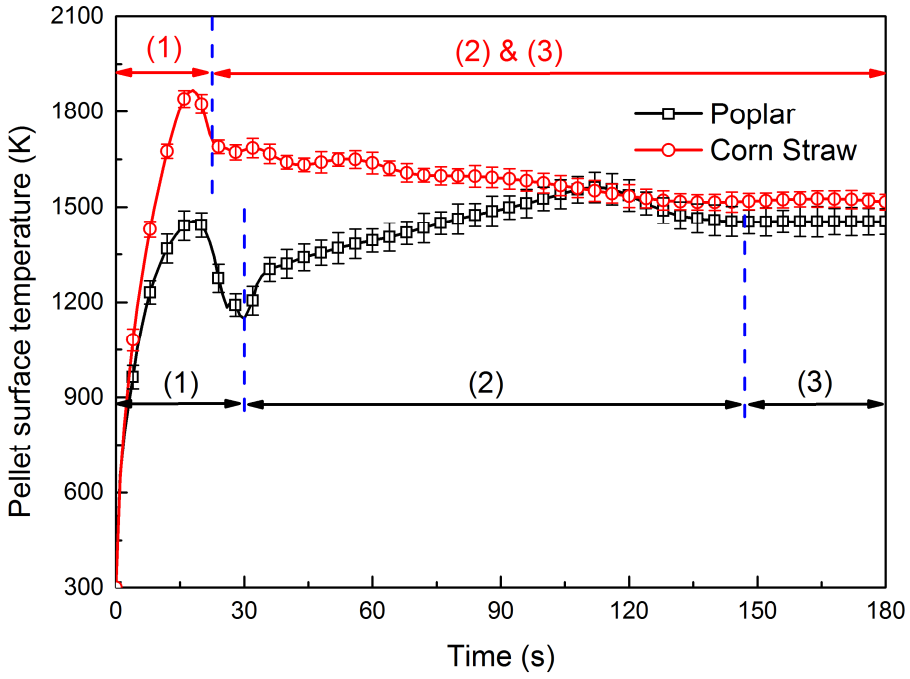

234
235 Figure 3. Temporal profiles of the surface temperature of poplar and corn straw pellets.
236
237 Figure 4 shows the temporal variation of the pellet diameter of poplar and corn straw during the
238 combustion. It can be found the pellets experience a continuous and smooth shrinking process during
239 all the three combustion stages. At the end of the experiments, the diameter of the corn straw pellet
240 reduces to 0.87 mm, while that of the poplar pellet becomes too small to be measured. This is because
241 poplar has an extremely low content of ash, i.e., only 2.3%.

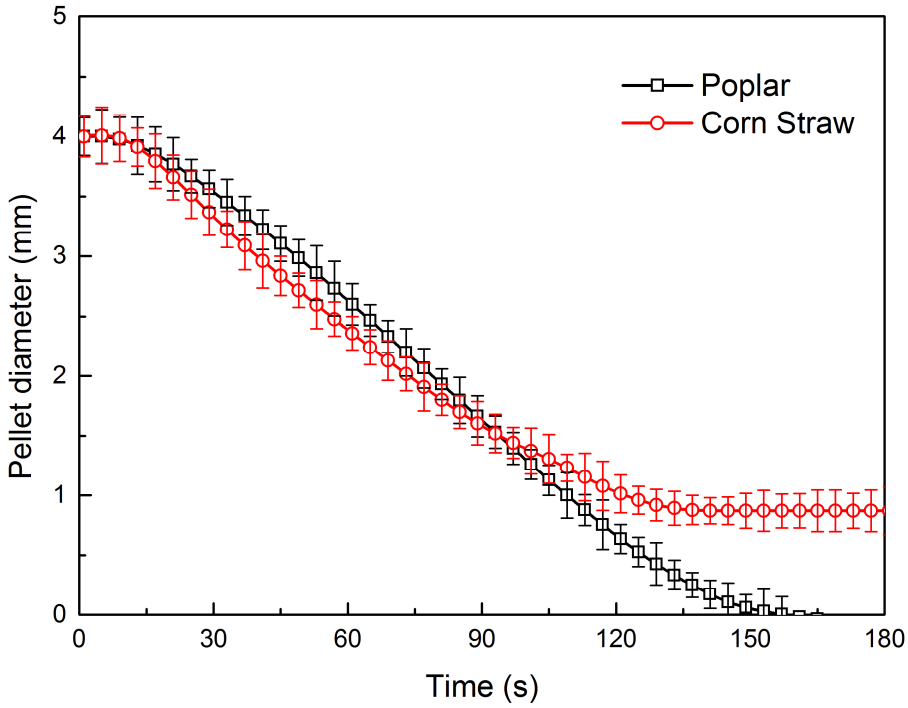

Figure 4. Temporal profiles of the diameters of the poplar and corn straw pellets.

To further analyze the correlation between the potassium release, temperature and diameter of the biomass pellets, the derivatives of the surface temperature and pellet diameter, i.e., dT/dt and dD/dt are plotted in Fig. 5. The potassium concentration in the gas phase measured by LIBS in Fig. 2 can be viewed as the derivative of the potassium content of the solid-fuel pellet. It can be observed that dT/dt experiences strong oscillations in the first 40 s for both poplar and corn straw during the highly active devolatilization and early char-burning stages, and then it becomes smooth for the residual time period. In contrast, the derivative of the pellet diameter dD/dt show a much smoother variation. It remains a stable value around -0.03 during almost the whole char-burning stage of poplar from 30 s to 120 s, which indicates the shrinking of the poplar pellet during the char burnout stage follows a linear trend. For corn straw, the profile of dD/dt is a single- and wide-peak distribution, indicating the oxidization rate gradually decreases during the char-burning stage. The time corresponding to the maximum potassium release rate is given by a dashed vertical line on the plots. It can be observed for both poplar

and corn straw, dT/dt changes from a positive to a negative value at this time, which indicates the maximum pellet surface temperature is achieved. Since the devolatilization rate of biomass reaches its maximum value at this time, the measured potassium concentration and the thermal effect of volatile combustion both reach their peaks.

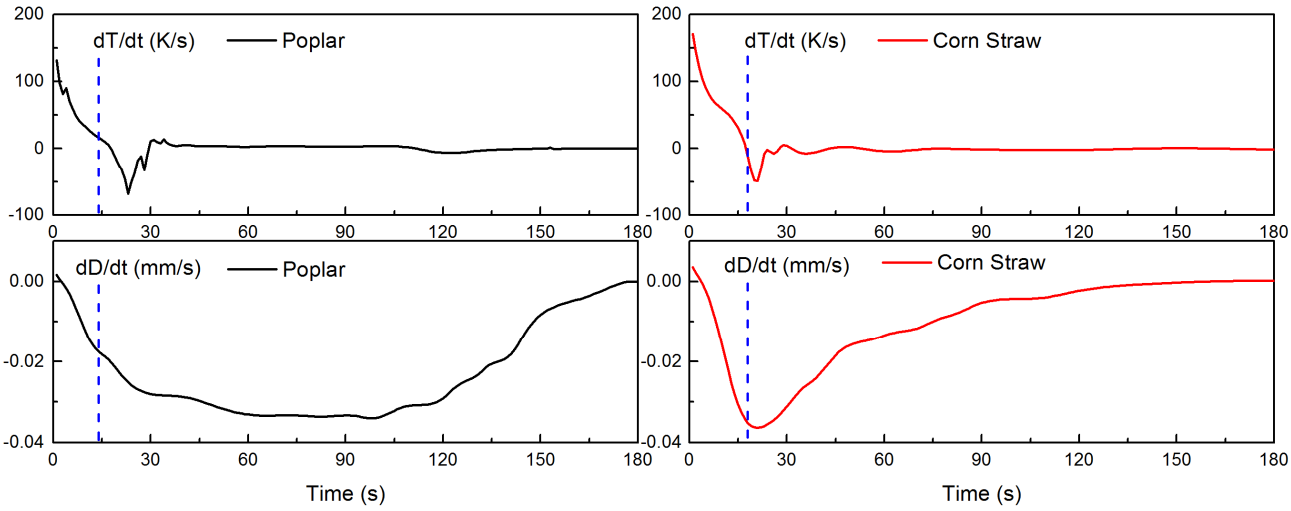

Figure 5. Temporal profiles of the derivatives of the surface temperature and diameter of the poplar and corn straw pellets. The dashed vertical line illustrates the time when the maximum potassium release rate is achieved.

3.2. Release characteristics of different chemical forms of potassium

Figure 6 shows the mass content of different chemical forms of potassium in poplar and corn straw. The mass of different chemical forms of potassium (mg) in a biomass pellet sample prepared from 1g of the raw poplar or corn straw was determined by performing ICP-AES on the filtrate obtained from each step of the chemical extraction, as detailed in Section 2.2. It can be observed that the major chemical form of potassium in both poplar and corn straw is H_2O-soluble potassium, which accounts for 52% and 90% of the total potassium mass in poplar and corn straw, respectively. The HCl-soluble potassium is marginal, accounting for less than 4% of the total potassium mass in both

biomass samples. The residual potassium is evenly distributed in NH_4Ac-soluble and insoluble forms for both poplar and corn straw.

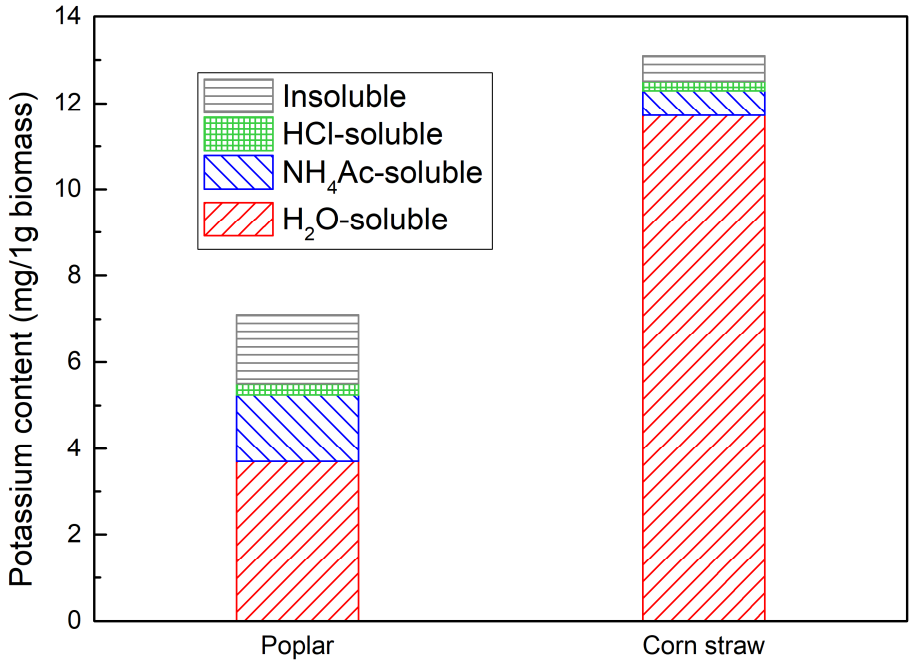

Figure 6. Content of different chemical forms of potassium in poplar and corn straw measured by ICP-AES.

Figure. 7 shows temporal potassium release profiles of pulverized poplar/corn straw pellets which were sequentially treated with H_2O, NH_4Ac and HCl. The difference between the potassium release profiles of the raw and H_2O-treated biomass illustrates the contribution of H_2O-soluble potassium in the total potassium release. Similarly, the contribution of NH_4Ac-soluble and HCl-soluble potassium compounds can be obtained from the difference between other two adjacent profiles, as illustrated in Fig. 7. The profiles of HCl-treated biomass represent the release of insoluble potassium. Obviously, H_2O-soluble potassium is the major potassium compound released during the combustion of the two biomass samples. After the biomass pellet is treated with H_2O and therefore H_2O-soluble potassium is removed, the potassium concentration detected by LIBS is largely decreased, especially for corn straw.

The removal of H_2O-soluble potassium also affects the char burnout stage of poplar. As shown in Fig. 7(a), the second peak of the H_2O-treated profile is delayed compared to that of the raw poplar, indicating the combustion of the pellet slows down. This is similar to our previous findings on the sodium release of a burning coal pellet [39], which were attributed to catalytic effects of alkali metal on accelerating the combustion of char. The potassium release characteristics of H_2O-, NH_4Ac- and HCl-treated biomass follow a similar trend to that of the corresponding raw biomass, but with a lower magnitude of potassium concentration. Finally, insoluble potassium is found to be released mainly during the first devolatilization stage, which can be explained by the fact that insoluble-potassium micro-particles generated inside the porous structure of the biomass pellet will be transported outward by the volatile vapor generated during the devolatilization stage [41]. It should be noted that the chemical fractionation treatment could change the properties, e.g., porous structure, of the biomass samples, and therefore their combustion characteristics may be affected which in turn influence the potassium release characteristics.

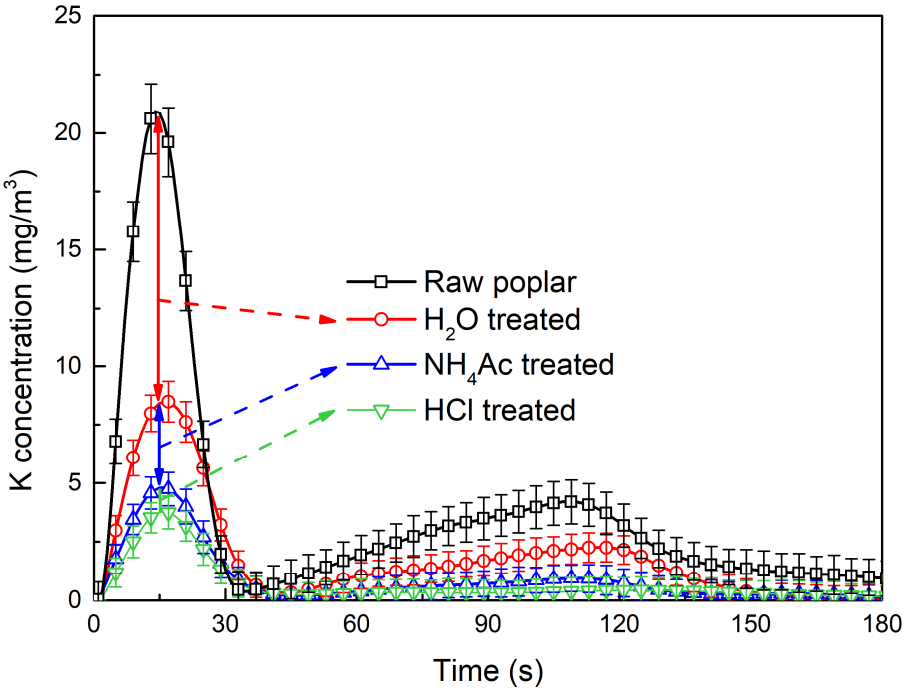

(a) Poplar

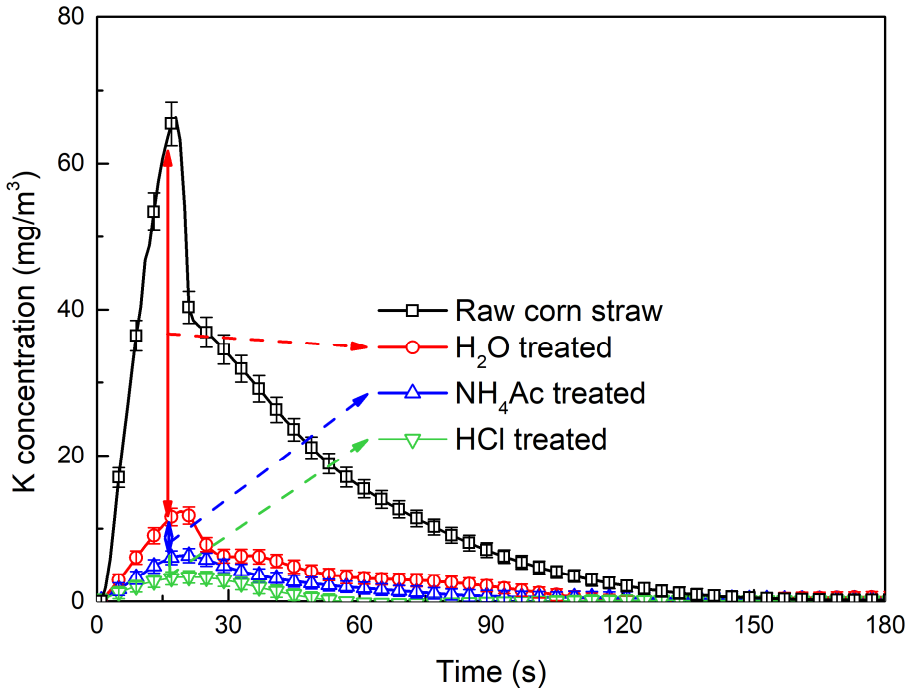

(b) Corn straw

Figure 7. Temporal potassium release profiles of poplar and corn straw sequentially treated with H_2O, NH_4Ac and HCl. The potassium release profiles of raw poplar and raw corn straw are also presented as a reference.

Figure 8 summarizes the release ratio of different chemical forms of potassium during the combustion of poplar and corn straw. ICP-AES was applied to the ashes of burned raw and H_2O-, NH_4Ac- and HCl-treated biomass pellets to obtain the residual potassium mass in the ash. By comparing it with the potassium mass in unburned raw and H_2O-, NH_4Ac- and HCl-treated biomass pellets, the release ratio of different chemical forms of potassium can be determined. It can be observed that the release ratio of H_2O-, NH_4Ac- and HCl-soluble potassium is relatively high, i.e., > 80% for both poplar and corn straw; while that of insoluble potassium is lower and between 55–68%. The release ratio reflects the release capability of different chemical forms of potassium. Specifically, H_2O-, NH_4Ac- and HCl-soluble potassium compounds have a stronger release capability than insoluble potassium during the combustion of the two biomass samples.

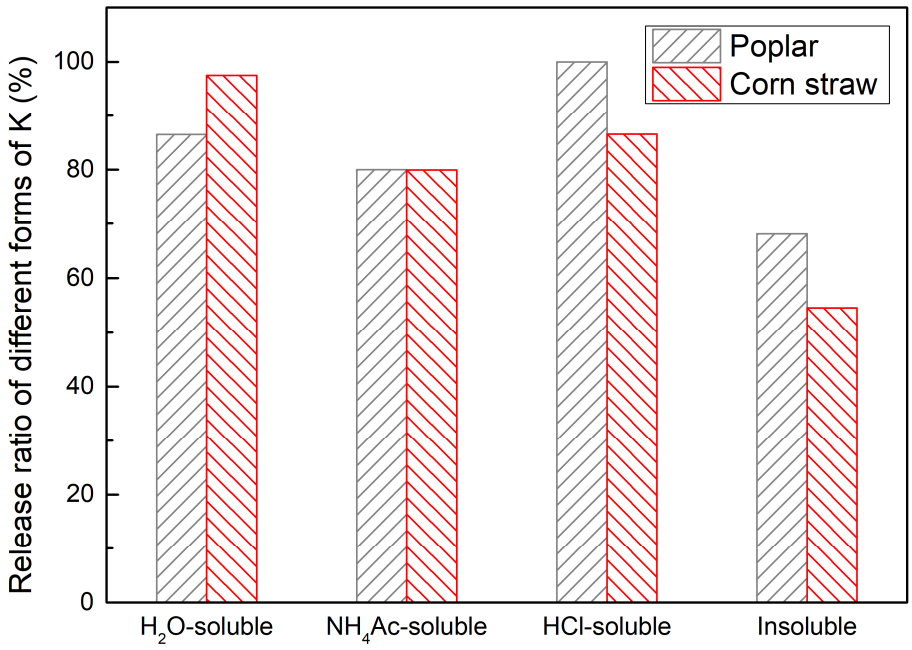

Figure 8. Release ratio of different chemical forms of potassium during the combustion of poplar and corn straw.

3.3. Inhibition effects of different additives on potassium release

A kind of additive was mixed with the biomass pellets of poplar and corn straw at a dosing ratio of 3% to investigate the inhibition effects of the additive on potassium release. Two pure additives, i.e., silica and alumina, and two natural mineral additives, i.e., kaolin and mica, were used in the present study. Figure 9 shows the temporal potassium release profiles of poplar and corn straw pellets mixed with one of the four additives. Compared against the potassium release profiles of the raw biomass pellets, all the four additives are found to be able to significantly reduce the release of potassium during the combustion. Specifically, silica and alumina show a similar inhibition characteristic: the potassium release in the first devolatilization stage is largely prohibited, while the inhibition effect during the char burnout stage is moderate. For the natural mineral additives, kaolin shows a strong potassium inhibition capability during the char burnout and ash cooking stages, while its performance during the first devolatilization stage is not as good as the natural additives. Considering the potassium release

during the devolatilization stage is mainly due to the evaporation and thermal decomposition of inorganic potassium while in the char burnout stage the decomposition of organic potassium plays a dominate role [20], the above findings indicate that kaolin's retention effects on inorganic potassium are limited while silica and alumina have difficulties to retain organic potassium. Finally, mica shows the best potassium inhibition performance among the four additives during the entire process of biomass burning.

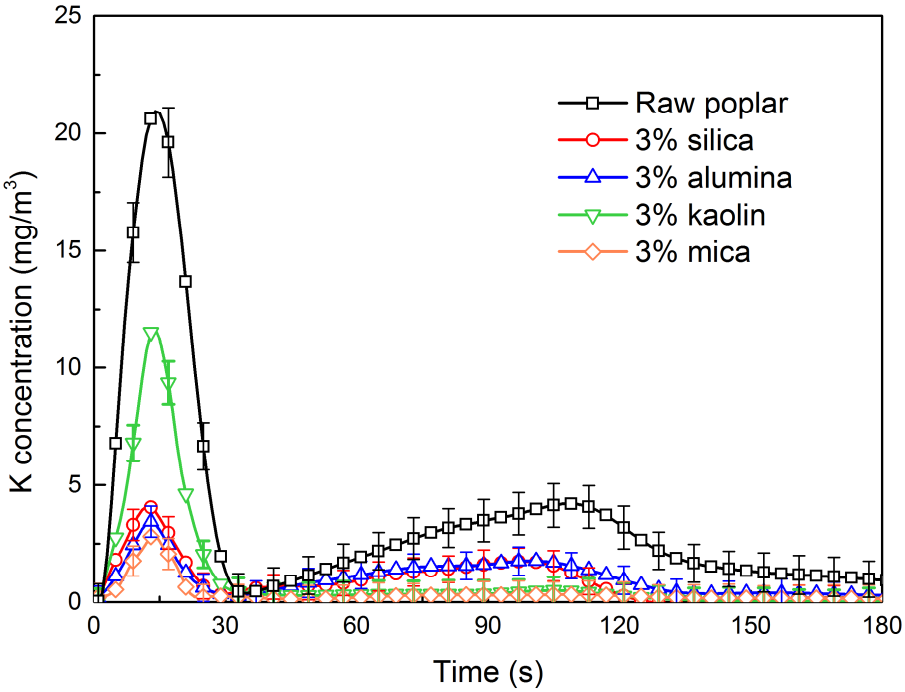

(a) Poplar

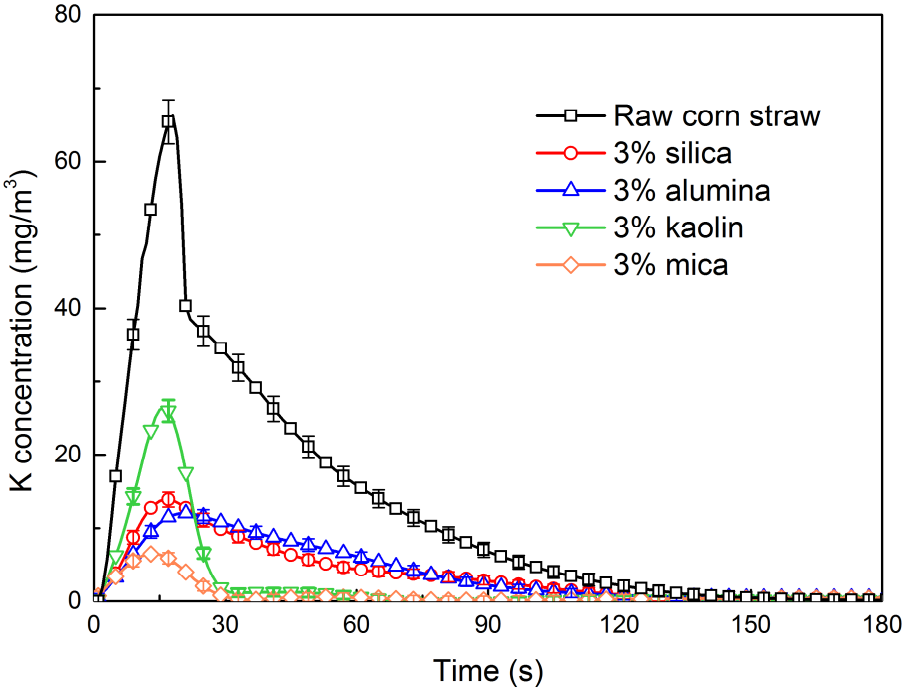

(b) Corn straw

Figure 9. Temporal potassium release profiles of raw biomass and biomass samples with 3% additives of silica, alumina, kaolin and mica.

By performing ICP-AES to the ashes of those blended biomass-additives, the potassium release amount of each case can be calculated. Comparing these data with the potassium release amount of the raw biomass samples, the inhibition efficiency of the four additives on potassium release can then be obtained. As shown in Fig. 10, all the four additives achieve an inhibition efficiency higher than 65%, which indicates the additive approach can be an effective way to control potassium emissions during biomass combustion. The performance of the four additives on the two different types of biomass is consistent. The natural minerals have a better inhibition performance than the pure additives. Although kaolin's inhibition performance is the worst in the devolatilization stage, it achieves an overall higher inhibition efficiency than silica and alumina because the duration of the char burnout stage is much longer than the devolatilization stage. Mica is found to have the highest inhibition efficiency (90%) for both poplar and corn straw.

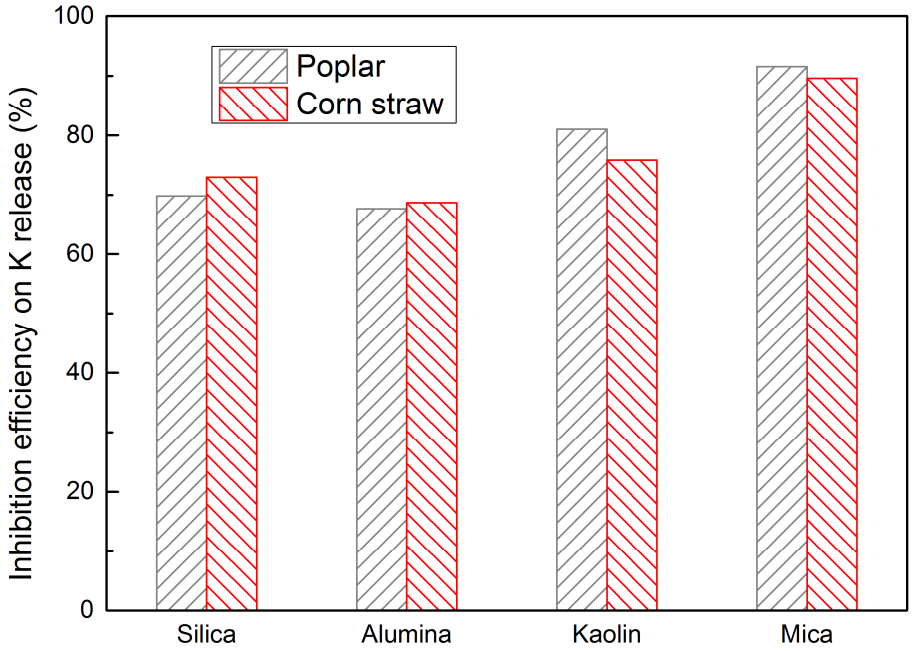

Figure 10. Efficiency of four additives, i.e., silica, alumina, kaolin and mica, on reducing potassium release during the combustion of poplar and corn straw.

4. Conclusions

Potassium release and its interaction with inhibitive additives during the combustion of a poplar/corn straw pellet have been studied using a combination of online LIBS and offline ICP measurements. A dual-peak potassium release characteristic is observed for poplar while only a single peak is found for corn straw. The strongest potassium release is found in the first devolatilization stage for both biomass samples.

The release characteristics of different chemical forms of potassium are then measured by LIBS for the biomass samples sequentially treated with H_2O, NH_4Ac and HCl. H_2O-soluble potassium is found to be the major released potassium compound. The corresponding ICP-AES analyses show that the release ratios of H_2O-, NH_4Ac- and HCl-soluble potassium are relatively high, i.e., > 80% for both poplar and corn straw; while that of insoluble potassium is lower and between 55–68%.

The inhibition effects of two pure additives, i.e., silica and alumina, and two natural mineral additives, i.e., kaolin and mica, on potassium release during biomass pellet combustion are studied. All the four additives achieve an inhibition efficiency higher than 65%, indicating the additive approach can be an effective way to control potassium emissions during biomass combustion. The natural minerals have a better inhibition performance than the pure additives, and mica is found to have the highest inhibition efficiency (90%) for both poplar and corn straw.

Acknowledgements

This work was jointly supported by the National Natural Science Foundation of China (51706200, 51776185, 51706059), the China Postdoctoral Science Foundation (2019M650136, 2019TQ0277). Kaidi Wan would also like to acknowledge the support by the Centre national de la recherche scientifique (CNRS) of the France.

References

[1] Hosseini SE, Wahid MA. Utilization of palm solid residue as a source of renewable and sustainable energy in Malaysia. Renewable and Sustainable Energy Reviews 2014;40:621-32.

[2] Niu Y, Tan H, Hui Se. Ash-related issues during biomass combustion: Alkali-induced slagging, silicate melt-induced slagging (ash fusion), agglomeration, corrosion, ash utilization, and related countermeasures. Prog. Energy Combust. Sci. 2016;52:1-61.

[3] Liu Y, Cheng L, Zhao Y, Ji J, Wang Q, Luo Z, et al. Transformation behavior of alkali metals in high-alkali coals. Fuel Process. Technol. 2018;169:288-94.

[4] Capablo J. Formation of alkali salt deposits in biomass combustion. Fuel Process. Technol. 2016;153:58-73.

[5] Liu YZ, He Y, Wang ZH, Xia J, Wan KD, Whiddon R, et al. Characteristics of alkali species release from a burning coal/biomass blend. Appl. Energy 2018;215:523-31.

406 [6] Fagerström J, Steinvall E, Boström D, Boman C. Alkali transformation during single pellet
407 combustion of soft wood and wheat straw. Fuel Process. Technol. 2016;143:204-12.
408 [7] Paneru M, Babat S, Maier J, Scheffknecht G. Role of potassium in deposit formation during wood
409 pellets combustion. Fuel Process. Technol. 2016;141:266-75.
410 [8] Capablo J, Ballester J. Experimental study of the kinetics of sulfation of alkali chloride deposits.
411 Fuel Process. Technol. 2015;140:215-21.
412 [9] Ma T, Fan C, Hao L, Li S, Jensen PA, Song W, et al. Biomass ash induced agglomeration in
413 fluidized bed. Part 2: Effect of potassium salts in different gas composition. Fuel Process. Technol.
414 2018;180:130-9.
415 [10] Wan KD, Xia J, Vervisch L, Liu YZ, Wang ZH, Cen KF. Modelling alkali metal emissions in
416 large-eddy simulation of a preheated pulverised-coal turbulent jet flame using tabulated chemistry.
417 Combust. Theory Model. 2018;22(2):203-36.
418 [11] Mason PE, Jones JM, Darvell LI, Williams A. Gas phase potassium release from a single particle
419 of biomass during high temperature combustion. Proc. Combust. Inst. 2017;36(2):2207-15.
420 [12] Mason PE, Darvell LI, Jones JM, Williams A. Observations on the release of gas-phase potassium
421 during the combustion of single particles of biomass. Fuel 2016;182:110-7.
422 [13] Weng W, Costa M, Aldén M, Li Z. Single particle ignition and combustion of pulverized pine
423 wood, wheat straw, rice husk and grape pomace. Proc. Combust. Inst. 2019;37(3):2663-71.
424 [14] He Z, Lou C, Fu J, Lim M. Experimental investigation on temporal release of potassium from
425 biomass pellet combustion by flame emission spectroscopy. Fuel 2019;253:1378-84.
426 [15] Weng W, Gao Q, Wang Z, Whiddon R, He Y, Li Z, et al. Quantitative Measurement of Atomic
427 Potassium in Plumes over Burning Solid Fuels Using Infrared-Diode Laser Spectroscopy. Energy
428 Fuels 2017;31(3):2831-7.
429 [16] Qu Z, Holmgren P, Skoglund N, Wagner DR, Broström M, Schmidt FM. Distribution of
430 temperature, H2O and atomic potassium during entrained flow biomass combustion – Coupling
431 in situ TDLAS with modeling approaches and ash chemistry. Combust. Flame 2018;188:488-97.
432 [17] Sorvajärvi T, DeMartini N, Rossi J, Toivonen J. In Situ Measurement Technique for Simultaneous
433 Detection of K, KCl, and KOH Vapors Released during Combustion of Solid Biomass Fuel in a
434 Single Particle Reactor. Appl. Spectrosc. 2014;68(2):179-84.
435 [18] Erbel C, Mayerhofer M, Monkhouse P, Gaderer M, Spliethoff H. Continuous in situ measurements

of alkali species in the gasification of biomass. Proc. Combust. Inst. 2013;34(2):2331-8.

[19] Hsu L-J, Alwahabi ZT, Nathan GJ, Li Y, Li ZS, Aldén M. Sodium and Potassium Released from Burning Particles of Brown Coal and Pine Wood in a Laminar Premixed Methane Flame Using Quantitative Laser-Induced Breakdown Spectroscopy. Appl. Spectrosc. 2011;65(6):684-91.

[20] Liu YZ, Wang ZH, Xia J, Vervisch L, Wan KD, He Y, et al. Measurement and kinetics of elemental and atomic potassium release from a burning biomass pellet. Proc. Combust. Inst. 2019;37(3):2681-8.

[21] Tchoffor PA, Moradian F, Pettersson A, Davidsson KO, Thunman H. Influence of Fuel Ash Characteristics on the Release of Potassium, Chlorine, and Sulfur from Biomass Fuels under Steam-Fluidized Bed Gasification Conditions. Energy Fuels 2016;30(12):10435-42.

[22] Zhang Z, Liu J, Shen F, Dong Y. Insights into the Effects of Atmosphere and Chlorine on Potassium Release during Biomass Combustion: Temporal Measurement and Kinetic Studies. Energy Fuels 2018;32(12):12523-31.

[23] Wan K, Wang Z, Xia J, Vervisch L, Domingo P, Lv Y, et al. Numerical study of HCl and SO2 impact on sodium emissions in pulverized-coal flames. Fuel 2019;250:315-26.

[24] Deng L, Ye J, Jin X, Che D. Transformation and release of potassium during fixed-bed pyrolysis of biomass. Journal of the Energy Institute 2018;91(4):630-7.

[25] Wan KD, Wang ZH, Xia J, Vervisch L, Domingo P, Lv Y, et al. Numerical study of HCl and SO2 impact on potassium emissions in pulverized-biomass combustion. Fuel Process. Technol. 2019;193:19-30.

[26] Fatehi H, Li ZS, Bai XS, Aldén M. Modeling of alkali metal release during biomass pyrolysis. Proc. Combust. Inst. 2017;36(2):2243-51.

[27] Cao W, Martí-Rosselló T, Li J, Lue L. Prediction of potassium compounds released from biomass during combustion. Appl. Energy 2019;250:1696-705.

[28] Deng L, Zhang T, Che D. Effect of water washing on fuel properties, pyrolysis and combustion characteristics, and ash fusibility of biomass. Fuel Process. Technol. 2013;106:712-20.

[29] Clery DS, Mason PE, Rayner CM, Jones JM. The effects of an additive on the release of potassium in biomass combustion. Fuel 2018;214:647-55.

[30] Steenari BM, Karlfeldt Fedje K. Addition of kaolin as potassium sorbent in the combustion of wood fuel – Effects on fly ash properties. Fuel 2010;89(8):2026-32.

[31] He Y, Whiddon R, Wang ZH, Liu YZ, Zhu YQ, Liu JZ, et al. Inhibition of Sodium Release from Zhundong Coal via the Addition of Mineral Additives: Online Combustion Measurement with Laser-Induced Breakdown Spectroscopy (LIBS). Energy Fuels 2017;31(2):1082-90.

[32] Liu YZ, Wang ZH, Lv Y, Wan KD, He Y, Xia J, et al. Inhibition of sodium release from Zhundong coal via the addition of mineral additives: A combination of online multi-point LIBS and offline experimental measurements. Fuel 2018;212:498-505.

[33] Smith GP, Golden DM, Frenklach M, Moriarty NW, Eiteneer B, Goldenberg M, et al. GRI-Mech 3.0. (http://www.me.berkeley.edu/gri_mech/).

[34] He Y, Zhu JJ, Li B, Wang ZH, Li ZS, Aldén M, et al. In-situ measurement of sodium and potassium release during oxy-fuel combustion of lignite using laser-induced breakdown spectroscopy: effects of O2 and CO2 concentration. Energy Fuels 2013;27(2):1123-30.

[35] Liu YZ, He Y, Wang ZH, Wan KD, Xia J, Liu JZ, et al. Multi-point LIBS measurement and kinetics modeling of sodium release from a burning Zhundong coal particle. Combust. Flame 2018;189:77-86.

[36] Huang Y, Yan Y, Riley G. Vision-based measurement of temperature distribution in a 500-kW model furnace using the two-colour method. Measurement 2000;28(3):175-83.

[37] DeWitt DP, Nutter GD. Theory and practice of radiation thermometry. Wiley Online Library; 1988.

[38] van Eyk PJ, Ashman PJ, Alwahabi ZT, Nathan GJ. Simultaneous measurements of the release of atomic sodium, particle diameter and particle temperature for a single burning coal particle. Proc. Combust. Inst. 2009;32(2):2099-106.

[39] Liu YZ, Wang ZH, Wan KD, Lv Y, Xia J, He Y, et al. In Situ Measurements of the Release Characteristics and Catalytic Effects of Different Chemical Forms of Sodium during Combustion of Zhundong Coal. Energy Fuels 2018;32(6):6595-602.

[40] Wang ZH, Liu YZ, Whiddon R, Wan KD, He Y, Xia J, et al. Measurement of atomic sodium release during pyrolysis and combustion of sodium-enriched Zhundong coal pellet. Combust. Flame 2017;176:429-38.

[41] Wan KD, Vervisch L, Xia J, Domingo P, Wang ZH, Liu YZ, et al. Alkali metal emissions in an early-stage pulverized-coal flame: DNS analysis of reacting layers and chemistry tabulation. Proc. Combust. Inst. 2019;37(3):2791-9.

Figure captions

Figure 1. LIBS measurement setup.

Figure 2. Temporal potassium release profiles of poplar and corn straw measured by LIBS. The three combustion stages of the biomass pellets are: (1) devolatilization, (2) char burnout, and (3) ash cooking.

Figure 3. Temporal profiles of the surface temperature of poplar and corn straw pellets.

Figure 4. Temporal profiles of the diameters of the poplar and corn straw pellets.

Figure 5. Temporal profiles of the derivatives of the surface temperature and diameter of the poplar and corn straw pellets. The dashed vertical line illustrates the time when the maximum potassium release rate is achieved.

Figure 6. Content of different chemical forms of potassium in poplar and corn straw measured by ICP-AES.

Figure 7. Temporal potassium release profiles of poplar and corn straw sequentially treated with H_2O, NH_4Ac and HCl. The potassium release profiles of raw poplar and raw corn straw are also presented as a reference.

Figure 8. Release ratio of different chemical forms of potassium during the combustion of poplar and corn straw.

Figure 9. Temporal potassium release profiles of raw biomass and biomass samples with 3% additives of silica, alumina, kaolin and mica.

Figure 10. Efficiency of four additives, i.e., silica, alumina, kaolin and mica, on reducing potassium release during the combustion of poplar and corn straw.

Color figures can be used for the online PDF version and the gray style for hardcopy reproduction.